Cell Calcium 80 (2019) 46–55

Contents lists available at ScienceDirect

Cell Calcium

journal homepage: www.elsevier.com/locate/ceca

Analyzing the structural and functional roles of residues from the 'black' and 'gray' clusters of human S100P protein

Maria E. Permyakova[a,*], Sergei E. Permyakov[a,b,*], Alexei S. Kazakov[a,b,1], Alexander I. Denesyuk[a,c], Konstantin Denessiouk[c,d], Vladimir N. Uversky[a,e,**], Eugene A. Permyakov[a,b,1]

[a] Institute for Biological Instrumentation of the Russian Academy of Sciences, Pushchino, Moscow region, 142290, Russia
[b] Department of Biomedical Engineering, Pushchino State Institute of Natural Sciences, Pushchino, Moscow region, 142290, Russia
[c] Structural Bioinformatics Laboratory, Biochemistry, Faculty of Science and Engineering, Åbo Akademi University, Turku, 20520, Finland
[d] Pharmaceutical Sciences Laboratory, Pharmacy, Faculty of Science and Engineering, Åbo Akademi University, Turku, 20520, Finland
[e] Department of Molecular Medicine, USF Health Byrd Alzheimer's Research Institute, Morsani College of Medicine, University of South Florida, Tampa, FL, 33612, USA

ARTICLE INFO

Keywords:
S100P
Clusters
Structure
Function
Order
Disorder

ABSTRACT

Two highly conserved structural motifs observed in members of the EF-hand family of calcium binding proteins. The motifs provide a supporting scaffold for the Ca2+ binding loops and contribute to the hydrophobic core of the EF-hand domain. Each structural motif represents a cluster of three amino acids called cluster I ('black' cluster) and cluster II ('grey' cluster). Cluster I is more conserved and mostly incorporates aromatic amino acids. In contrast, cluster II is noticeably less conserved and includes a mix of aromatic, hydrophobic, and polar amino acids of different sizes. In the human calcium binding S100 P protein, these 'black' and 'gray' clusters include residues F15, F71, and F74 and L33, L58, and K30, respectively. To evaluate the effects of these clusters on structure and functionality of human S100 P, we have performed Ala scanning. The resulting mutants were studied by a multiparametric approach that included circular dichroism, scanning calorimetry, dynamic light scattering, chemical crosslinking, and fluorescent probes. Spectrofluorimetric Ca2+-titration of wild type S100 P showed that S100 P dimer has 1–2 strong calcium binding sites ($K_1 = 4 \times 106\ M^{-1}$) and two cooperative low affinity ($K_2 = 4 \times 104\ M^{-1}$) binding sites. Similarly, the S100 P mutants possess two types of calcium binding sites. This analysis revealed that the alanine substitutions in the clusters I and II caused comparable changes in the S100 P functional properties. However, analysis of heat- or GuHCl-induced unfolding of these proteins showed that the alanine substitutions in the cluster I caused notably more pronounced decrease in the protein stability compared to the changes caused by alanine substitutions in the cluster II. Opposite to literature data, the F15 A substitution did not cause the S100 P dimer dissociation, indicating that F15 is not crucial for dimer stability. Overall, similar to parvalbumins, the S100 P cluster I is more important for protein conformational stability than the cluster II.

1. Introduction

Calcium-binding proteins, which are grouped into several large families [1,2], play important roles in practically all biological processes. One of the most studied families of calcium-binding proteins is the EF-hand protein superfamily (reviewed in [2]). The EF-hand

Abbreviations: CD, circular dichroism spectroscopy; DSC, differential scanning calorimetry; DTT, DL-dithiothreitol; EDTA, ethylenediaminetetraacetic acid; EGTA, ethylene glycol-bis2-aminoethylether-N,N,N',N'-tetraacetic acid; ESI-MS, electrospray ionization mass spectrometry; HEPES, N-(2-hydroxyethyl)piperazine-N'-(2-ethanesulfonic acid); rWT S100P, recombinant wild-type S100P; PMSF, phenylmethanesulfonyl fluoride; SDS-PAGE, sodium dodecyl sulfate polyacrylamide gel electrophoresis; Tris, tris(hydroxymethyl) amino methane

* Corresponding authors at: Institute for Biological Instrumentation of the Russian Academy of Sciences Federal Research Center "Pushchino Scientific Center for Biological Research of the Russian Academy of Sciences", Institutskaya str., 7, Pushchino, Moscow region, 142290, Russia.
** Corresponding author at: Department of Molecular Medicine, Morsani College of Medicine, University of South Florida, Tampa, FL, 33612, USA.
E-mail addresses: permyakova-masha@rambler.ru (M.E. Permyakova), permyakov.s@gmail.com (S.E. Permyakov), vuversky@health.usf.edu (V.N. Uversky).
[1] Institute for Biological Instrumentation of the Russian Academy of Sciences Federal Research Center "Pushchino Scientific Center for Biological Research of the Russian Academy of Sciences", Institutskaya str., 7, Pushchino, Moscow region, 142290, Russia.

https://doi.org/10.1016/j.ceca.2019.03.008
Received 21 February 2019; Received in revised form 26 March 2019; Accepted 27 March 2019
Available online 28 March 2019

calcium binding domain consists of two helices and a calcium-binding loop between them [3–5]. The EF-hand domains in Ca^{2+} binding proteins are usually paired. Most of the EF-hand family members, such as calmodulin and troponin C, function as Ca^{2+}-dependent sensor proteins. Others, mostly parvalbumin and calbindin, seem to serve as cytosolic Ca^{2+} buffers [6].

Examination of representative tertiary structures of the EF-hand containing proteins from eleven structural subfamilies revealed the presence of noticeable structural nonequivalence of the individual EF-hands in the paired EF-hand domain [7]. We found two highly conserved structural motifs, which provide a supporting scaffold for the Ca^{2+} binding loops and contribute to the hydrophobic core of the EF-hand domain [7]. Each structural motif forms a cluster of three amino acids. These clusters were called cluster I ('black' cluster) and cluster II ('grey' cluster). Cluster I ('black') is much more conserved and mostly consists of aromatic amino acids. It lacks destabilizing interactions and has a predominant aromatic mini-core that is stabilized by a set of linked CH-π and CH—O hydrogen bonds [7]. We suggested that cluster I is likely vital for structural stabilization of the EF-hand domain in its critical gate region, where the polypeptide chain enters and exits the domain. In contrast, cluster II includes a mix of aromatic, hydrophobic, and polar amino acids of different sizes. It is less conserved, lacks stabilizing interactions, and its residues are more often engaged in destabilizing interactions [7]. We suggested that the higher variability of cluster II ('gray') could promote adaptation to the conformational and dynamic requirements imposed by the need to ensure wide range of kinetic and equilibrium metal binding constants, as well as recognition of various targets (proteins, lipids and so on). The analysis of the structures of clusters I and II and of their rearrangements in response to Ca^{2+} binding enabled to propose a more detailed classification of the EF-hand proteins, different from their classical division on metal sensors and buffers [7]. Obviously, structural and functional significance of the discovered 'black' and 'grey' clusters in calcium-binding proteins requires experimental support.

In our previous work [8], we studied the 'black' and 'gray' clusters in rat β-parvalbumin that included residues F48, A100, and F103 and G61, L64, and M87, respectively. In that study, we sequentially substituted these amino acid residues by Ala, except Ala100, which was substituted by Val. Physical properties of the mutants were studied by circular dichroism, scanning calorimetry, dynamic light scattering, chemical crosslinking, and fluorescent probes. The Ca^{2+} and Mg^{2+} binding affinities of these mutants were evaluated by intrinsic fluorescence and equilibrium dialysis methods [8]. It was found that the alanine substitutions in the cluster I of rat β-parvalbumin caused noticeably more pronounced changes in various structural and conformational properties of the proteins, such as hydrodynamic radii of their apo-forms, thermal stability of Ca^{2+}/Mg^{2+}-loaded forms, and total energy of Ca^{2+} binding in comparison with the changes caused by similar amino acid substitutions in the cluster II. These findings were further supported by the results of computational analysis of the effects of these mutations on the intrinsic disorder predisposition of rat β-parvalbumin, which also indicated that local intrinsic disorder propensities and the overall levels of predicted disorder were strongly affected by mutations in the cluster I, whereas mutations in cluster II had less pronounced effects [8]. These results demonstrated that amino acids of the cluster I in rat β-parvalbumin provide more essential contribution to the maintenance of the structural integrity and functional properties of the protein in comparison with the residues of the cluster II [8]. The present work is devoted to the experimental evaluation of the structural and functional roles of the 'black' and 'grey' clusters in a representative of the S100 P protein subfamily.

S100 proteins constitute a large subfamily of the superfamily of the EF-hand calcium-binding proteins (reviewed by [9,10]). S100 proteins are the smallest members of the EF-hand superfamily and their molecules consist of only two EF-hand domains. Acidic amino acid residues within the Ca^{2+}-binding loop provide ligands for Ca^{2+} binding in a pentagonal bipyramidal fashion. The C-terminal EF-hand of S100 proteins is canonical and binds calcium with relatively high affinity, possessing the equilibrium dissociation constant, K_d, that ranges from 10 to 50 μM (reviewed by [9,10]). The N-terminal EF-loop has two more residues (14 instead of 12) in comparison with the canonical EF-hand, and therefore it has lower affinity to calcium. Most of the S100 proteins form stable symmetric homodimers. S100 proteins regulate many intracellular and extracellular activities including protein phosphorylation and enzyme activity, gene transcription, dynamics of cytoskeleton components, and cell proliferation and differentiation (reviewed by [9,10]).

For our studies, we have chosen one of the members of the S100 family, S100 P, a 95-amino-acid protein first extracted from placenta [11,12]. Expression of S100 P was found in various cancer cell lines, and there is accumulating evidence that it is overexpressed in a number of solid tumors. For example, S100 P protein seems to play a significant role in development and progression of different cancers (reviewed in [9,10]). In fact, increased levels of S100 P have been observed in multiple tumor cell lines and breast, pancreas, lung and ovary carcinomas (reviewed in [13]). A number of microarray and immunohistochemical studies have shown that S100 P transcription and protein expression correlate with the characteristic features of malignant phenotype in various types of tissues (reviewed in [14]).

According to the literature data, S100 P protein has two Ca^{2+}-binding sites; one with high affinity (canonical) (K_d 1.6 μM) and the other one with lower affinity (non-canonical) (K_d 800 μM) [11]. The secondary structure of the S100 P protein is only insignificantly affected by the binding of calcium but its tertiary structure is altered considerably resulting in an exposure of hydrophobic surfaces [15,16], and this is related to the homodimer formation [17]. Furthermore, these calcium-induced conformational changes activate the protein and render a conformation that is capable of binding other proteins.

S100 P exists as a homodimer, structure of which is supported by the non-covalent interactions between the large hydrophobic areas of protomers [18]. Conserved hydrophobic amino acid residues involved in dimerization of S100 P have been identified [19]. This study revealed that F15 is crucially important for dimerization, since its substitution by alanine abolished dimerization [19]. A replacement of I11, I12, or F89 by less hydrophobic residues in both subunits of S100 P also resulted in serious disturbance of the dimerization [19]. It was also shown that the association kinetics of S100 P dimers is faster in the presence of calcium ions than in their absence, whereas dissociation rate constant is independent of calcium [18]. Equilibrium dissociation constant values for S100 P dimers are 64 nM and 2.5 μM in the presence and in the absence of calcium ions, respectively [18].

2. Materials and methods

2.1. Materials

Molecular biology grade HEPES, ultra-grade H_3BO_3 and BioUltra-grade glycine were from Calbiochem, Fluka, and Sigma-Aldrich Co, respectively. Ultra-pure grade Tris, high pure-grade PMSF and ultra-pure grade Tricine were purchased from Amresco. Biotechnology grade DTT was bought from DiaM (Moscow, Russia). Biochemistry grade guanidinium chloride (GuHCl) was a product of Merck. USP grade sodium chloride, molecular mass markers for SDS-PAGE, were from Helicon (Moscow, Russia). Analytical grade bis-ANS was purchased from Sigma-Aldrich Co. DEAE-Sephacel resin, Phenyl Sepharose 6 Fast Flow resin were from Amersham Biosciences. Sephadex G-25 was product of Pharmacia LKB. Standard solutions of calcium chloride and magnesium chloride (Ca^{2+} content of 0.0005%), ultra-grade EDTA and EGTA were from Sigma-Aldrich Co, EDAC and Sulfo-NHS were from Bio-Rad. Other chemicals were reagent grade or higher.

All buffers and other solutions were prepared using ultrapure water (Millipore Simplicity 185 system). Plastic or quartz ware was used

instead of glassware, to avoid contamination of protein samples with Ca^{2+}. Thermo SnakeSkin dialysis tubing (3.5 kDa MWCO) was used for dialysis of protein solutions.

2.2. Methods

2.2.1. Mutagenesis, isolation and purification of human S100 P and its mutants

Alanine scanning of the residues comprising black (F15, F71, F74) and grey (K30, L33, L58) clusters [20] of human S100 P was performed. The pET-11a (Novagen) plasmid encoding wild-type human S100 P (kindly provided by Dr. Roger Barraclough, University of Liverpool, UK) was subjected to site-directed mutagenesis [21] resulting in F15 A, F71 A, F74 A, K30 A, L33 A and L58 A mutants. The S100 P cluster mutants were expressed and purified as previously described [22].

The human S100 P and its mutant samples were homogeneous as judged by SDS-PAGE. Their UV absorption and fluorescence spectra were characteristic for Tyr residues. Protein concentration was estimated spectrophotometrically using molar extinction coefficient $\varepsilon_{280nm} = 2980\ M^{-1}\ cm^{-1}$ determined according to [23]. The yield was 40–60 mg of protein per liter of cell culture. The presence of Met1 residue in the wild-type S100 P and its mutants was confirmed by electrospray ionization mass spectrometry (ESI-MS).

2.2.2. Preparation of apo-proteins

Human S100 P and its mutants (3.2 mM) in 10 mM glycine-KOH, 5 mM EDTA, pH 9.2 buffer were decalcified by passage through a Sephadex G-25 column (1 cm × 20 cm) (0.3 mL; 0.25 mL/min) equilibrated with a buffer [24] of choice. 10 mM HEPES-KOH, pH 7.3 was used for dynamic light scattering measurements and chemical crosslinking experiments; 10 mM HEPES-KOH, pH 7.3 was used for measurements of calcium affinity; 10 mM Tricine-KOH, pH 7.4 was used for circular dichroism measurements and Bis-ANS fluorescence.

2.2.3. Chemical crosslinking of S100P

Distribution of recombinant wild type human S100 P and its mutants over oligomeric forms was studied by chemical crosslinking method. Crosslinking of human S100 P and its mutants (30 μM) with EDAC/Sulfo-NHS was performed in 10 mM HEPES-KOH, pH 7.3. Metal-depleted forms of S100Ps were prepared using the Sephadex G-25 gel-filtration method [24]. 1 mM $CaCl_2$ was added to obtain Ca^{2+}-loaded proteins. The reaction proceeded for 2 h at 20 °C and was stopped by addition of 4-fold volume of the buffer used in SDS-PAGE electrophoresis in the presence of 100 mM DTT. The samples were subjected in SDS-PAGE (5% concentrating and 18% resolving gels; 5 μg of S100Ps per lane) and stained with Coomassie Brilliant Blue R-250. The gels were scanned using Molecular Imager Pharos FX Plus System (Bio-Rad Laboratories, Inc.) and analyzed by Quantity One software.

2.2.4. Scanning calorimetry measurements

Differential scanning calorimetry (DSC) studies were carried out on a Nano DSC microcalorimeter (TA Instruments) at a 1 K/min heating rate and excess pressure of 4 bar. Wild-type human S100 P and its mutant concentrations were 1.5–2.0 mg/ml. Buffer conditions: 10 mM H_3BO_3-KOH, 1 mM $CaCl_2$, pH 9.0 (Ca^{2+}-loaded proteins); 20 mM glycine-KOH, 1 mM EDTA, pH 9.2 (apo-proteins). The DSC measurements and calculations of protein specific heat capacity (C_p) were performed as described in [25]. The partial molar volume of S100 P and specific heat capacity of the fully unfolded protein were estimated according to [26] and [27], respectively. The experimental data were fitted by the equations derived earlier [28] using Microcal OriginPro 8.0 (Origin Lab Corporation, Northampton, MA, USA) software. The heat capacity change accompanying the thermal transition (ΔC_p) was supposed to be independent of temperature. Heat capacity change ΔC_p, mid-transition temperature (T_m), enthalpy of protein denaturation at temperature T_m (ΔH_0), and n were used as fitting parameters (in some cases n was set to 1).

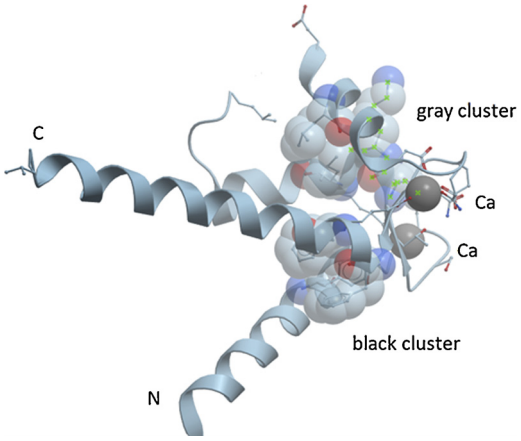

Fig. 1. Tertiary structure of Ca^{2+}-loaded (PDB code 1J55) monomer human S100 P protein. Bound calcium ions and residus of the 'black' and 'gray' clusters are shown.

2.2.5. Circular dichroism measurements

Circular dichroism (CD) studies were carried out with a J-810 spectropolarimeter (JASCO, Inc.), equipped with a Peltier-controlled cell holder. The instrument was calibrated with an aqueous solution of d-10-camphorsulfonic acid according to the manufacturer's instruction. The cell compartment was purged with nitrogen (dew point of –40 °C). The quartz cell with the path-length of 1.00 mm was used for far-UV region measurements. Protein concentration was 9.4–10 μM. Buffer conditions: 10 mM Tricine-KOH, 1 mM EDTA, pH 7.4; 10 mM Tricine-KOH, 1 mM $CaCl_2$, pH 7.4, (for apo- and Ca^{2+}-loaded S100 P states, respectively) or 10 mM Tricine-KOH, 1 mM EGTA-KOH, 1 mM $MgCl_2$, pH 7.4 (for Mg^{2+}-loaded S100 P); 20 °C. A small contribution of buffer was subtracted from the experimental spectra. Band width was 2 nm, averaging time 2 s, and accumulation 3. The spectra were analyzed in the 200–240 nm range using CDPro software package [29] (http://lamar.colostate.edu/~sreeram/CDPro/main.html). SELCON3, CDSSTR, and CONTIN algorithms were used for evaluation of the secondary structure fractions. SDP48 and SMP56 reference protein sets were used for these evaluations. The final secondary structure fractions represent averaged values. Apo-forms of S100 P and its mutants were prepared using the gel-filtration method described by [24] in the presence of 5 mM EDTA.

2.2.6. Dynamic light scattering studies

Dynamic light scattering (DLS) measurements were carried out at 15 °C using a Zetasizer Nano ZS system (Malvern Instruments Ltd.). The backscattered light from a 4 mW He-Ne laser (632.8 nm) was collected at an angle of 173°. Human S100 P and its mutants concentration was 1.5 mg/ml. Before the measurements the protein samples were passed through 0.02 μm Whatman Anotop 10 syringe filters. The buffer conditions were 20 mM H_3BO_3-KOH, pH8.4, 1.5 mM EDTA (for apo-proteins), 1 mM $CaCl_2$ (for Ca^{2+}-loaded proteins). Acquisition time for a single autocorrelation function was 100 s. The resulting autocorrelation functions were averaged values from ten measurements. The estimates of mean hydrodynamic radii of the proteins were derived from these distributions. Apparent molecular weights of S100 P and its mutants were calculated by the equation [30]:

$$\log(Rs) = -(0.254) + (0.369) \times \log(MW) \quad (1)$$

2.2.7. Fluorescence measurements

Fluorescence studies were performed with a Cary Eclipse spectrofluorimeter (Varian, Inc.), equipped with a Peltier-controlled cell

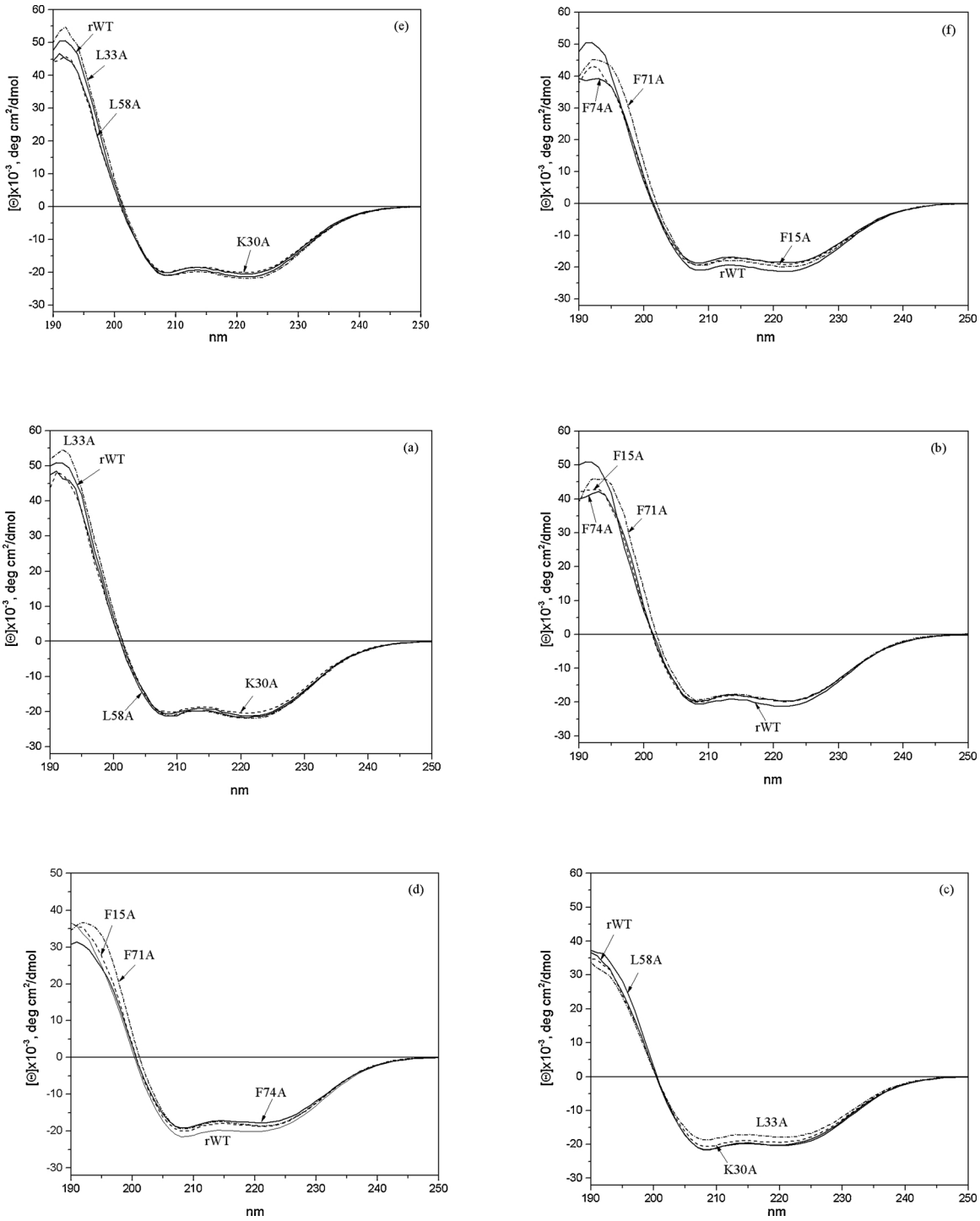

Fig. 2. Far-UV CD spectra of apo- (1 mM EDTA) (a and b correspond to mutants with mutations in the 'gray' and 'black' clusters, respectively), Ca^{2+}- (1 mM $CaCl_2$) (c and d correspond to mutants with mutations in the 'gray' and 'black' clusters, respectively) and Mg^{2+}- loaded (1 mM EGTA-KOH, 1 mM $MgCl_2$) (e and f correspond to mutants with mutations in the 'gray' and 'black' clusters, respectively) forms of recombinant human S100 P and its cluster mutants at 20 °C. 10 mM Tricine-KOH, pH 7.4.

holder. Quartz cells with the path-length of 10 mm were used. Protein concentrations were 9–10 μM. Fluorescence of Tyr residues of S100 P was excited at 280 nm. Bis-ANS concentration was estimated spectrophotometrically using molar extinction coefficient at 385 nm 16.790 $M^{-1}\,cm^{-1}$ [31]. Bis-ANS fluorescence was excited at 385 nm. Buffer conditions for experiments with bis-ANS: 10 mM Tricine-KOH, pH 7.4, 1 mM EDTA or 1 mM $CaCl_2$ for apo- and Ca^{2+}-loaded proteins, respectively, or 10 mM Tricine-KOH, pH 7.4, 1 mM EGTA, 1 mM $MgCl_2$ for Mg^{2+}-loaded form. Concentrations of S100 P and bis-ANS were 10 μM and 1 μM, respectively. Maximum intensity (*I*max) and maximum position (λmax) of fluorescence emission spectra were obtained from fits of the spectra with log-normal curves [32] using LogNormal software (IBI RAS, Pushchino).

2.2.8. Measurements of Ca^{2+} binding constants

Ca^{2+} binding to S100 P protein and its mutants was studied by the intrinsic fluorescence method. The binding of Ca^{2+} ions to wild type S100 P and some of its mutants was described by the following Ca^{2+}-

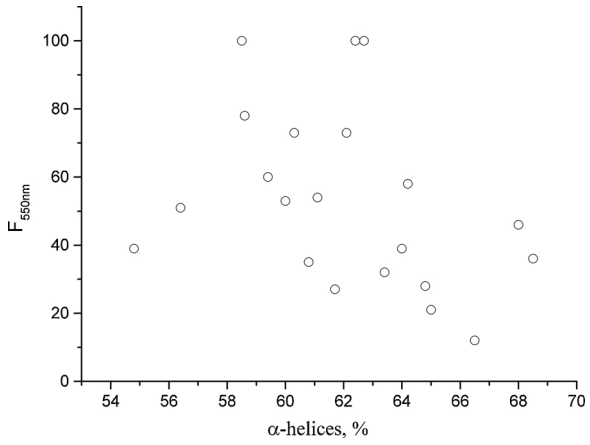

Fig. 3. Correlation between α-helical content and fluorescence intensity at 500 nm of bound bis-ANS fluorescent probe for the whole collection of the wild type human S100 P and its cluster mutants under the variety of conditions.

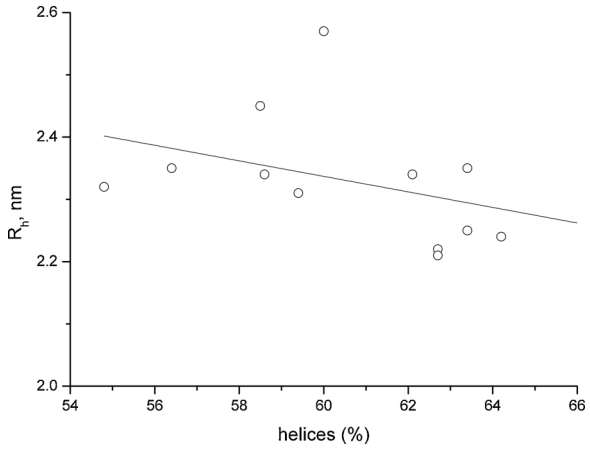

Fig. 4. Correlation between α-helical content and hydrodynamic radius for the whole collection of the wild type human S100 P and its cluster mutants under the variety of conditions.

binding scheme, which suggests the existence in a protein of a single strong binding site (binding constant K_1) and n lower affinity cooperative binding sites with effective binding constant K_2 (a justification for the use of this scheme see below):

$$K_1\ P + Ca^{2+} \leftrightarrow P{\cdot}Ca,\ K_2\ P{\cdot}Ca + nCa^{2+} \leftrightarrow P{\cdot}Ca_{n+1}, \quad (1)$$

The calcium affinity of S100 P and its mutants was estimated from a spectrofluorometric titration of the Ca^{2+}-free protein with a $CaCl_2$ standard. The experimental data were fitted using FluoTitr v.1.2 software [28,33]. The fit was achieved by variation of the binding constants K_1, K_2 and n. The quality of the fit was judged by the randomness of residuals distribution. The resulting accuracy of the determination the Ca^{2+}-binding constant K_1 was about ± 1.5 orders of their magnitude, while the accuracy of the determination of K_2 was about ± 0.5 orders of their magnitude.

2.2.9. Measurements on GuHCl-induced unfolding of rWT S100 P and its cluster mutants

GuHCl-induced denaturation of Ca^{2+} - loaded rWT human S100 P and its mutants monitored by intrinsic tyrosine fluorescence at 304 nm. S100 P and its cluster mutants stock solutions were prepared in 10 mM HEPES-KOH, 1 mM $CaCl_2$, pH7.3. Stock solution of 6.5 M GuHCl was made in 10 mM HEPES-KOH, pH7.3. A series of solutions containing a fixed amount of S100 P and its mutants (3 μM) and varying concentrations of GuHCl (0–6 M) were prepared from the stock solutions. The final volume of each sample was 1 ml. The solutions were allowed to sit for at least 1 h and the fluorescence spectrum of each sample was then measured. The extitation wavelength was 280 nm and the fluorescence emission spectrum was recorded over the wavelength range from 290 to 340 nm. All experiments were done at 25 °C. The experimental data were fitted by a sigmoidal curve, and the concentration of the mid-transition was used as a measure of protein stability.

2.3. Computational evaluation of the intrinsic disorder predisposition of human S100 P protein and its cluster mutants

The intrinsic disorder of human S100 P protein (UniProt ID: P25815) and its F15 A, F71 A, and F74 A (black cluster) and K30 A, L33 A, and L58 A (gray cluster) and were evaluated by several disorder predictors, such as PONDR® VSL2 [34] (which is one of the more accurate stand-alone disorder predictors [34–36]), PONDR® VL3 [37] (which is a tool for accurate evaluation of long intrinsically disordered regions), PONDR® VLXT [38] (a computational tool sensitive to the local sequence peculiarities that can be used for identification of disorder-based binding sites), IUPred platform [39] (that allow reliable evaluation of long and short disordered regions), and a metapredictor PONDR® FIT [40] (which is more accurate than each of its component predictors, PONDR® VLXT [38], PONDR® VSL2 [34], PONDR® VL3 [37], FoldIndex [41], and IUPred [39]). Outputs of these six tools were averaged to produce the mean disorder profiles for all the proteins analyzed in this study. The resulting mean disorder propensity for these proteins based on the averaging of disorder profiles of individual predictors represents a way to increase the increased predictive performance [36,40,42–46]. In these analyses, residues and regions are considered disordered or flexible if their predicted disorder scores are above 0.5 and between 0.2 and 0.5, respectively.

3. Results and discussion

The 'black' and 'gray' clusters in recombinant S100 P consist of residues F15, F71, and F74 and L33, L58, and K30, respectively (Fig. 1). We sequentially substituted all these amino acids by Ala. The resulting mutants were expressed in *E. coli* and their molecular masses were checked by means of mass spectrometry.

The effects of the cluster mutations on the secondary structure of S100 P were studied by means of circular dichroism method. Fig. 2 shows far-UV circular dichroism spectra of S100 P and its cluster mutants in apo (1 mM EDTA-KOH), Mg^{2+}-loaded (1 mM EGTA-KOH, 1 mM $MgCl_2$), and Ca^{2+}-loaded (1 mM $CaCl_2$) forms at 20 °C. Table 1S contains data on fractions of the secondary structure elements estimated from the CD spectra of these proteins (Fig. 2). Mutations in the 'black' and 'gray' clusters of S100 P can result both in a slight increase (1–5 %) or decrease (1–4 %) in the α-helical content of its apo-form. Earlier we revealed that in comparison with the recombinant wild type rat β-parvalbumin, all apo-forms of its cluster mutants had a *decreased* α-helical content, except A100 V and G61 A mutants, which were characterized by an increased α-helical content [8]. The Mg^{2+}-loaded forms of both 'black' and 'gray' cluster mutants of S100 P show mostly 2 to 5% decrease in the α-helical content and an increase in the contributions of other elements of secondary structure. About 1 to 2% increase in the α-helical content was found only for F71 A ('black' cluster) and L33 A ('gray' cluster) mutants. Similarly, Mg^{2+}-loaded forms of the mutant β-parvalbumin show 10 to 20% decrease in the α-helical content and an increase in the contributions of other secondary structure elements in comparison with the recombinant wild type rat β-parvalbumin [8]. In comparison with the Ca^{2+}-loaded form of recombinant wild type human S100 P, the calcium bound forms of the mutant proteins demonstrated mostly a decreased α-helical content. Only L33 A was characterized by an increase in the α-helical content. The contents of all other elements of secondary structure can be both slightly increased or decreased. In comparison with recombinant wild type rat β-

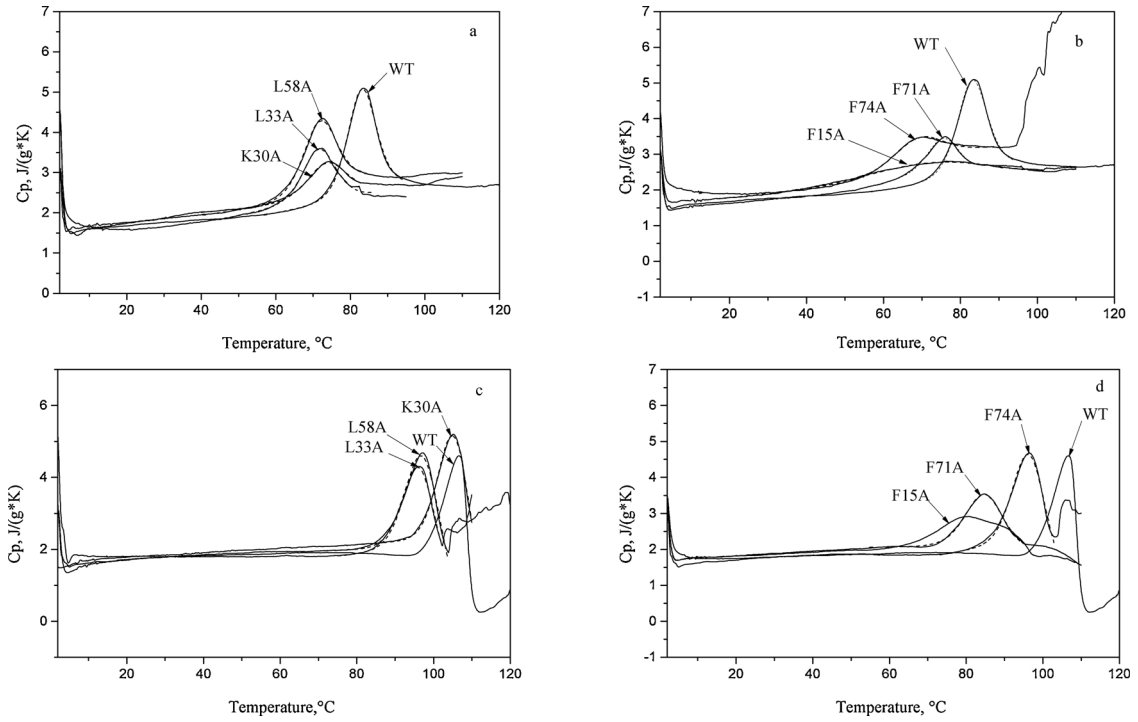

Fig. 5. Temperature dependencies of specific heat capacity for apo (10 мМ Glycine–KOH, 1 mM EDTA) - a, b and Ca^{2+}-loaded (10 mM H_3BO_3–KOH, pH 9.0; 1 mM $CaCl_2$) - c, d forms of recombinant human S100 P and its cluster mutants. Protein concentration 1.5–2.0 mg/ml.

parvalbumin, all calcium-bound forms of the mutant parvalbumins demonstrated 10 to 15% *decrease* in the α-helical content and increase in the contributions of other secondary structure elements, such as β-structure, turns, and unordered structures (2 to 7% each) [8]. Therefore, the mutations in the 'black' and 'gray' clusters cause only small changes in the secondary structure of S100 P protein. In many cases, the changes are on the verge of measurement accuracy (changes in α-helical content by 1% and less).

Structural compactness and the presence of solvent-exposed hydrophobic clusters of S100 P and its cluster mutants were studied by means of fluorescent probe bis-ANS. A transition of bis-ANS (and 8-ANS as well) from aqueous to hydrophobic environment (e.g., that of solvent-exposed hydrophobic clusters of proteins) results in a blue shift of its fluorescence maximum and in an increase of its fluorescence quantum yield (fluorescence intensity) ([47–49]; for review see [50]). Table 2S shows fluorescence parameters of bis-ANS bound to S100 P and its cluster mutants under variety of conditions. It is evident that the mutations in the 'black' and 'gray' clusters in most cases result in a decrease in protein compactness and hence in an increase in bis-ANS fluorescence intensity and in a blue shift of fluorescence spectrum maximum regardless of the metal binding state. At the same time, some mutations caused an increase in protein compactness and hence a decrease in bis-ANS fluorescence intensity. Fig. 3 shows a correlation between α-helical content and fluorescence intensity at 500 nm of bound bis-ANS fluorescent probe for the whole collection of the wild type human S100 P and its cluster mutants under the variety of conditions.

We have studied the oligomeric state of rWT S100 P and its mutants by chemical crosslinking and dynamic light scattering methods. The results of the chemical crosslinking and dynamic light scattering methods are presented in Table 3S and Fig. 1S (a–c). One can clearly see that apo- and Ca^{2+}-loaded forms of wild type S100 P are mostly in dimeric state with essential contribution of oligomers. The mutations in the 'black' and 'gray' clusters increase the contribution of dimers, eliminate oligomers and result in appearance of monomers and sometimes trimers. The origin of trimers is not clear at present. Earlier, it was found [19] that F15, which is a part of the 'black' cluster, is crucially important for the S100 P dimerization, since substitution of this residue by alanine abolishes dimerization. In that study, the interaction strength between the different S100 P chains, expressed as fusions with the binding or activation domain of Gal4, was evaluated by an indirect method measuring the expression level of the lacZ reporter gene [19]. However, according to our data obtained by more direct method of chemical crosslinking this mutation practically does not change the dimerization degree of calcium loaded S100 P and even increases dimer content of the apo-protein by 23% (Table 3S). These observations indicated that F15 is not crucial for the S100 P dimer formation.

Interestingly, the hydrodynamic radii R_h of the apo-states of the S100 P mutants were, as a rule, smaller than the hydrodynamic radii of their Ca^{2+}-loaded states. Apo-forms of β-parvalbumins with mutations in the 'black' cluster demonstrate noticeable *increase* in the hydrodynamic radius R_h (by 11–16 %) in comparison with that of the wild type protein, while the proteins with mutation in the 'gray' cluster were characterized by the noticeably smaller increase in R_h (by 4%), or even by a decrease in R_h, which means a decrease in the protein molecule volume [8]. The mutations in the 'black' cluster of β-parvalbumin always increased the hydrodynamic radius, while the mutations in the 'gray' cluster can both increase and decrease hydrodynamic radius of the protein. We did not find such regularity in the case of S100 P mutants, but such comparisons in this case are complicated by the large contribution of the wild type S100 P oligomers, which increases the effective R_h value. In contrast to β-parvalbumins, the mutations in both 'black' and 'gray' clusters of S100 P always decreased R_h.

Fig. 4 shows a correlation between the α-helical content and hydrodynamic radius for the whole collection of human S100 P forms. As in the case of β-parvalbumin [8], an increase in helical content is accompanied by a decrease in the hydrodynamic radius of a protein molecule, which seems to be quite logical.

Fig. 5 shows temperature dependencies of the specific heat capacity for apo- and Ca^{2+}-loaded forms of human S100 P and its cluster mutants measured by differential scanning calorimetry. The heat sorption peaks correspond to cooperative heat denaturation of the proteins.

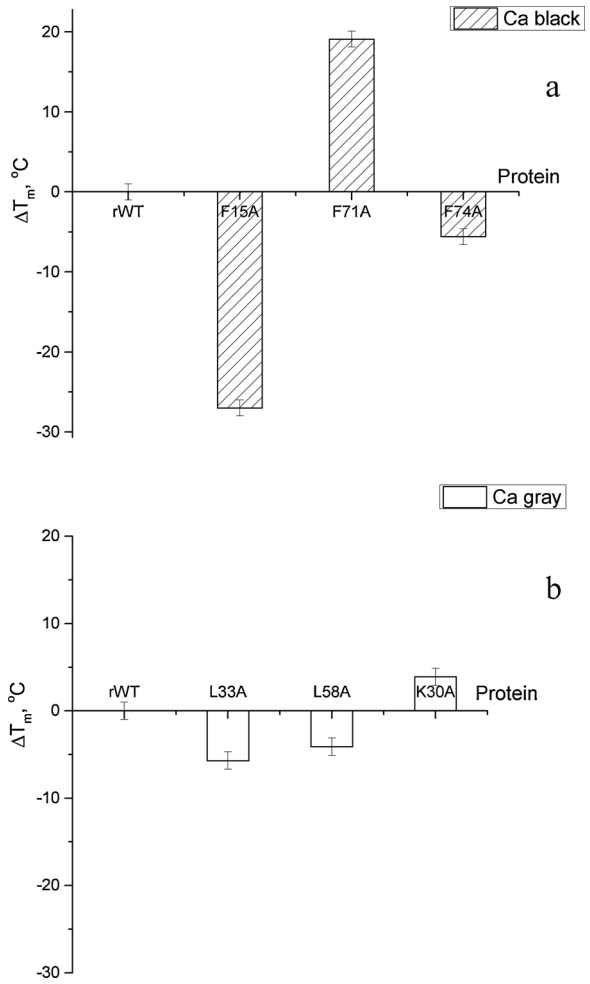

Fig. 6. Effects of cluster mutations on thermal transition mid-temperature of Ca^{2+}-loaded recombinant human S100P: **a** – mutations in the 'black' cluster; **b** – mutations in the 'gray' cluster. Vertical bars show accuracy of determination of T_m.

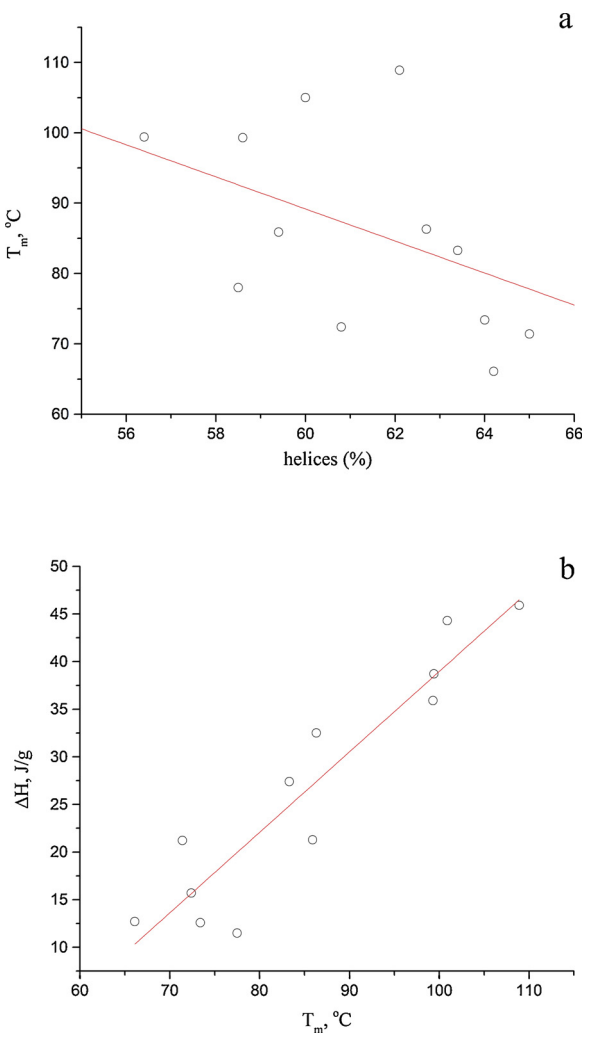

Fig. 7. a – Correlation between α-helical content and transition mid-temperature for the whole collection of the wild type human S100 P and its cluster mutants under the variety of conditions. **b** - Correlation between transition mid-temperature and transition enthalpy for the whole collection of the wild type human S100 P and its cluster mutants under the variety of conditions.

Table 4S lists thermodynamic parameters of the thermal denaturation of these proteins under the variety of conditions obtained from the corresponding differential scanning calorimetry data using the two-state model of thermal denaturation. These data show that the mutations in the 'black' and 'gray' clusters of S100 P caused mostly a decrease in the mid-transition temperature of both apo- and Ca^{2+}-loaded proteins (except apo-F15 A). Similar mutations in rat β-parvalbumin can cause both an increase and a decrease in the mid-transition temperature of the metal-loaded proteins [8]. It is of importance that, like in the case of rat β-parvalbumin [8], mean values of the absolute changes in thermal stability of Ca^{2+}-loaded S100 P proteins caused by alanine substitutions in the 'black' cluster were essentially more pronounced than those caused by the alanine substitutions in the 'gray' cluster (Fig. 6).

Fig. 7a shows a correlation between the α-helical content and the transition mid-temperature for the whole collection of the wild type and mutant S100Ps. Surprisingly, an increase in the α-helical content results in a *decrease* in the protein thermal stability. In the case of rat β-parvalbumin, an increase in the α-helical content resulted in more expected *increase* in the protein thermal stability [8]. Fig. 7b demonstrates that the increase in protein thermal stability is lineally related to the increase in thermal transition enthalpy.

We have also studied stability of rWT human S100 P and its cluster mutants to guanidine hydrochloride (GuHCl) induced unfolding. Fig. 8 shows GuHCl-induced unfolding curves for the Ca^{2+}-loaded

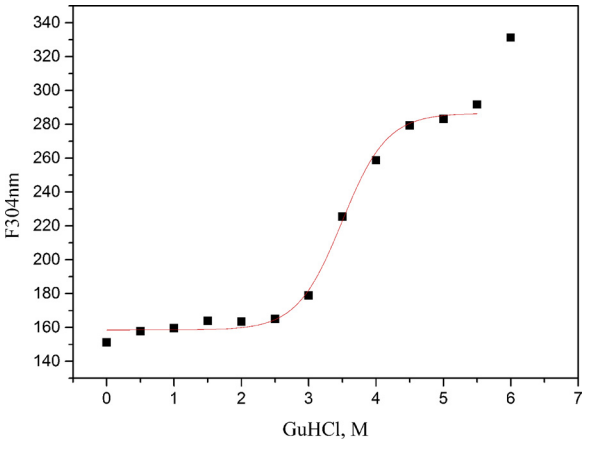

Fig. 8. GuHCl-induced denaturation of Ca^{2+}-loaded recombinant wild type S100 P protein monitored by intrinsic tyrosine fluorescence at 304 nm. Experimental data are fitted by a theoretical sigmoidal curve. 10 mM HEPES-KOH, pH7.3, 1 mM $CaCl_2$; protein concentration 3μM; 25 °C. Fluorescence was excited at 280 nm.

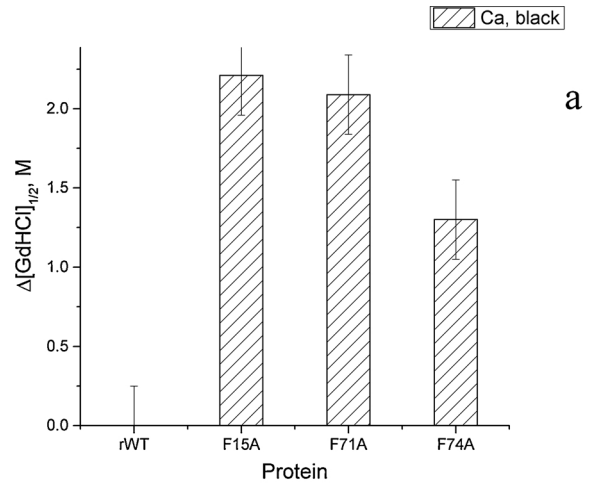

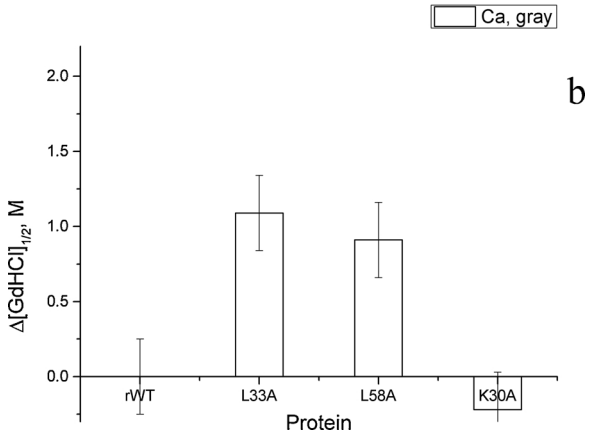

Fig. 9. Effects of the alanine substitutions on concentration of the GuHCl-induced denaturation transition in Ca^{2+}-loaded recombinant wild type S100 P. **a** – mutations in the 'black' cluster; **b** – mutations in the 'gray' cluster. 10 mM HEPES-KOH, pH7.3; 1 mM $CaCl_2$; 25 °C. Protein concentration 3 μM. Vertical bars show accuracy of determination of $[GdHCl]_{1/2}$.

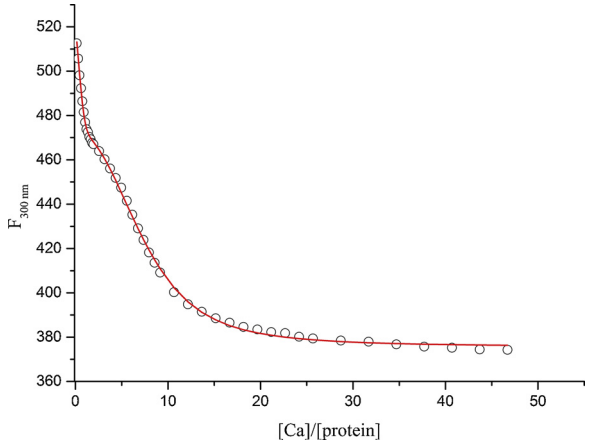

Fig. 10. Spectrofluorometric Ca^{2+}-titration of wild type human S100 P. 10 mM HEPES-KOH pH 7.3. Protein concentration 9–10 μM. Points are experimental data, whereas curve is a fit of these data to a theoretical curve computed according to the scheme [I].

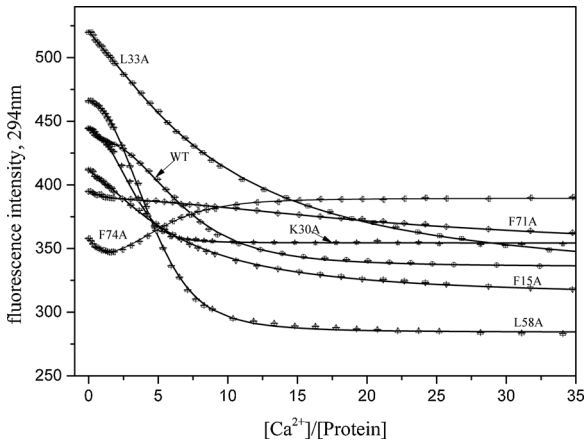

Fig. 11. Spectrofluorometric Ca^{2+}-titration of wild type human S100 P and its mutants. 10 mM HEPES-KOH pH 7.3. Protein concentration 9–10 μM. Points are experimental data, curves are best fits to theoretical curve computed according to the scheme [I].

recombinant wild type S100 P monitored by intrinsic tyrosine fluorescence as an example of such experiments. An increase in the GuHCl concentration caused a cooperative unfolding of the protein, which caused an increase in the tyrosine fluorescence intensity. The experimental data were fitted by a sigmoidal curve, and the concentration of the mid-transition was used as a measure of protein stability. Fig. 9 shows effects of the alanine substitutions in the 'black' (Fig. 9a) and 'gray' (Fig. 9b) clusters on the mid-position of the GuHCl-induced unfolding transitions for the Ca^{2+}-loaded recombinant wild type S100 P. Like in the case of thermal denaturation, the mutations in the 'black' cluster cause about two times more pronounced decrease in protein stability in comparison with the mutations in the 'gray' cluster. Similar effects were observed for the Ca^{2+}-free recombinant wild type S100 P and its cluster mutants.

Ca^{2+} binding is related to the physiological functions of S100 P. Fig. 10 shows results of the spectrofluorometric Ca^{2+}-titration of apo-state of wild type S100 P. The binding of calcium causes a decrease in the tyrosine fluorescence intensity. Fig. 10 shows that the titration curve consists of two region, where the first region corresponds to the binding of calcium ions to strong sites and the second one correspond to a cooperative binding of several (n) calcium ions to low affinity sites. For this reason, the binding of Ca^{2+} ions to wild type S100 P was described by the scheme [I], which suggests the existence in this protein of 1–2 strong calcium-binding sites (effective binding constant K_1) and n lower affinity cooperative binding sites with effective binding constant K_2. Our analysis revealed that the best fit of a theoretical curve computed according to the scheme [I] to experimental points for wild type S100 P is achieved when $K_1 = 3.5 \times 10^6$ M^{-1}; $K_2 = 3.8 \times 10^4$ M^{-1}; and n = 2.4.

Earlier, the binding of calcium to S100 P protein was analyzed using calcium buffers [51]. This study found that the S100 P molecule had at least two Ca^{2+}-binding sites with different affinity, where the high affinity binding site had an apparent binding constant of approximately 10^7 M^{-1} and the low affinity binding site possessed an apparent binding constant of approximately 10^4 M^{-1}, which is close to our results. According to results of this previous study, the high and low affinity Ca^{2+}-binding sites are located in the C- and N-terminal parts of the S100 P molecule, respectively.

Fig. 11 and Table 5S shows results of spectrofluorometric Ca^{2+}-titration of apo-state of recombinant wild type S100 P and its mutants. Like rWT S100 P, the proteins with the mutations in the 'black' and 'gray' clusters also possessed two types of calcium-binding sites. Unfortunately, the binding of Ca^{2+} to the strong sites caused rather small changes in the tyrosine fluorescence of these proteins, which did not

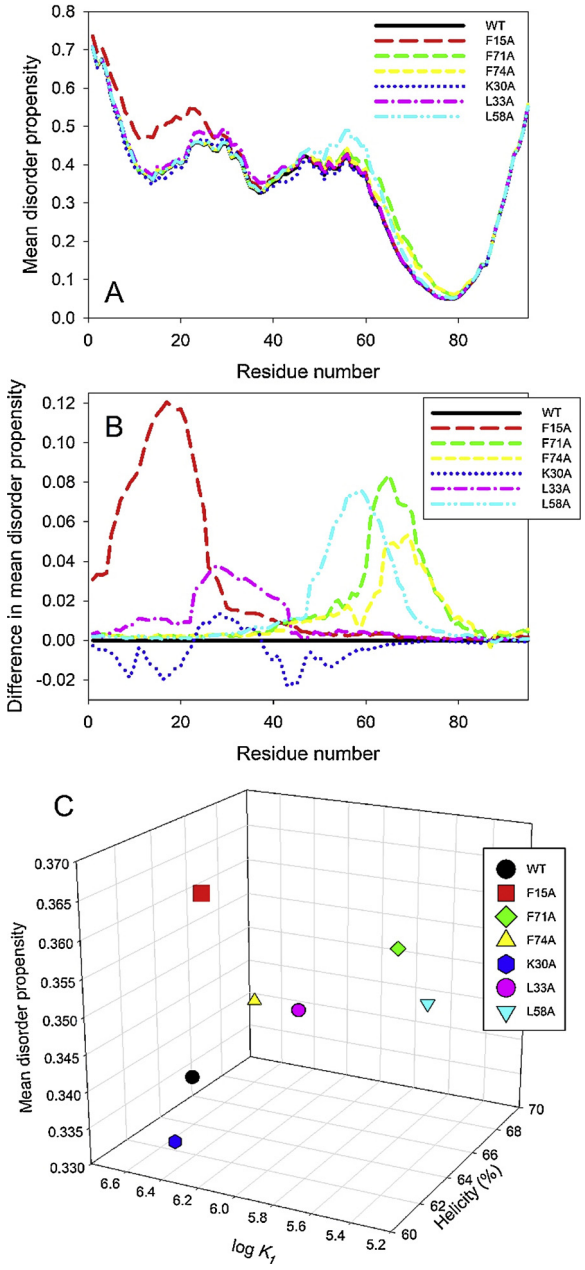

Fig. 12. Effect of cluster mutations on intrinsic disorder predisposition (A, B) and structural and functional properties of human S100 P (C). **Plot A** represents intrinsic disorder profiles of human S100 P protein and its cluster mutants in a form of the per-residue mean disorder propensity calculated for each protein by averaging disorder profiles of six individual predictors (PONDR® VLXT, PONDR® VL3, PONDR® VSL2, PONDR® FIT, IUPred_short, and IUPred_long). **Plot B** shows "difference disorder spectra" calculated by subtracting mean disorder profile of wild type S100 P from the mean disorder profiles of individual cluster mutants. In plot C, a correlation is shown between the protein-average disorder propensity, helical propensity, and equilibrium Ca^{2+} binding constants ($log\ K_1$) of human S100 P and its cluster mutants.

allow us to determine calcium-binding parameters with sufficient accuracy. Interestingly, the cooperative binding of Ca^{2+} to lower affinity sites of the F74 A mutant causes not a decrease but an *increase* in fluorescence intensity. We did not find any clear regularities in the effects of the mutations in 'black' and 'gray' clusters of human S100 P on its affinity to calcium. In the case of rat β-parvalbumin the alanine substitutions in the 'black' cluster cause noticeably more pronounced decrease in the Ca^{2+} affinity than analogous substitutions in the 'gray' cluster [8]. It is of interest that upon calcium titration tyrosine fluorescence of F71 A and F74 A mutants remains either unchanged or even increases, whereas in all other cases increase of calcium concentration is accompanied by a decrease of fluorescence. The sign of the calcium induced fluorescence change depends upon specific environment of the tyrosine chromophore, which can be different in different mutants.

To check if the cluster mutations (F15 A, F71 A, and F74 A (black cluster) and K30 A, L33 A, and L58 A (gray cluster)) affect the intrinsic disorder predisposition of human S100 P (UniProt ID: P25815), several commonly used disorder predictors, such as PONDR® VLXT, PONDR® VL3, PONDR® VSL2, PONDR® FIT, and the IUPred computational platform were used. Although for a given protein, each of these disorder predictors generates its own disorder profile, such predictor-specific per-residue disorder profiles were averaged to generate a mean per-residue intrinsic disorder profile for S100 P and its cluster mutants. Results of this analysis are summarized in Fig. 12A, whereas Fig. 12B shows "difference disorder spectra" calculated by the subtracting the mean disorder profile of the wild type S100 P from the disorder profiles of each of it cluster mutants. This analysis revealed that similar to the analogous data obtained earlier for the rat β-parvalbumin and its cluster mutants, the mutations in 'black' cluster caused more noticeable changes in the local disorder propensity in comparison to the effects of the 'gray' cluster mutations. Next, we compared cluster mutation-induced changes in the intrinsic disorder propensity of human S100 P with mutation-induced changes in helical propensity and equilibrium Ca^{2+} binding constants ($\boldsymbol{log}\ K_1$) of this protein (Fig. 12C). Similar to the results of the analogous analysis conducted earlier for rat β-parvalbumin, Fig. 12C shows that these three parameters correlate with each other relatively well, suggesting that the key-residues of 'black' and 'gray' clusters may play a role in the control of structure and function of human S100 P.

Conflict of interest statement

We, Maria E. Permyakova, Sergei E. Permyakov, Alexei S. Kazakov, Alexander I. Denesyuk, Konstantin A Denessiouk, Vladimir N. Uversky, and Eugene A. Permyakov, authors of the manuscript entitled "Analyzing the structural and functional roles of residues from the 'black' and 'gray' clusters of human S100 P protein", wish to confirm that there are no known conflicts of interest associated with this publication and there has been no significant financial support for this work that could have influenced its outcome.

Acknowledgements

This study was funded by the Russian Science Foundation (grant #16-14-10373 to E.A.P.).

Appendix A. Supplementary data

Supplementary material related to this article can be found, in the online version, at doi:https://doi.org/10.1016/j.ceca.2019.03.008.

References

[1] E.A. Permyakov, Metalloproteomics, John Wiley & Sons, Inc., Hoboken, New Jersey, 2009.
[2] E.A. Permyakov, R.H. Kretsinger, Calcium Binding Proteins, A John Wiley & Sons, Inc., Hoboken, New Jersey, 2011.
[3] C.E. Nockolds, R.H. Kretsinger, C.J. Coffee, R.A. Bradshaw, Structure of a calcium-binding carp myogen, Proc. Natl. Acad. Sci. U. S. A. 69 (1972) 581–584.
[4] R.H. Kretsinger, C.E. Nockolds, Carp muscle calcium-binding protein. II. Structure determination and general description, J. Biol. Chem. 248 (1973) 3313–3326.
[5] P.C. Moews, R.H. Kretsinger, Refinement of the structure of carp muscle calcium-binding parvalbumin by model building and difference Fourier analysis, J. Mol. Biol. 91 (1975) 201–225.
[6] E.A. Permyakov, Parvalbumin, Nova Science Publishers, New York, 2006.
[7] K. Denessiouk, S. Permyakov, A. Denesyuk, E. Permyakov, M.S. Johnson, Two structural motifs within canonical EF-Hand calcium-binding domains identify five

different classes of calcium buffers and sensors, PLoS One 9 (2014).
[8] S.E. Permyakov, A.A. Vologzhannikova, P.A. Khorn, M.P. Shevelyova, A.S. Kazakov, V.I. Emelyanenko, A.I. Denesyuk, K. Denessiouk, V.N. Uversky, E.A. Permyakov, Comprehensive analysis of the roles of' black' and' gray' clusters in structure and function of rat beta-parvalbumin, Cell Calcium 75 (2018) 64–78.
[9] R. Donato, S100: a multigenic family of calcium-modulated proteins of the EF-hand type with intracellular and extracellular functional roles, Int. J. Biochem. Cell Biol. 33 (2001) 637–668.
[10] R. Donato, C.L. Geczy, D.J. Weber, S100 proteins, in: R.H. Kretsinger, V.N. Uversky, E.A. Permyakov (Eds.), Encyclopedia of Metalloproteins, Springer Science +Business Media, New York, 2013, pp. 1863–1874.
[11] T. Becker, V. Gerke, E. Kube, K. Weber, S100P, a novel Ca(2+)-binding protein from human placenta. cDNA cloning, recombinant protein expression and Ca2+ binding properties, Eur. J. Biochem. 207 (1992) 541–547.
[12] Y. Emoto, R. Kobayashi, H. Akatsuka, H. Hidaka, Purification and characterization of a new member of the S-100 protein family from human placenta, Biochem. Biophys. Res. Commun. 182 (1992) 1246–1253.
[13] H.F. Jiang, H. Hu, X.M. Tong, Q.H. Jiang, H.Y. Zhu, S.Y. Zhang, Calcium-binding protein S100P and cancer: mechanisms and clinical relevance, J. Cancer Res. Clin. 138 (2012) 1–9.
[14] V. Tothova, A. Gibadulinova, S100P, a peculiar member of S100 family of calcium-binding proteins implicated in cancer, Acta Virol. 57 (2013) 238–246.
[15] P. Cancemi, G. Di Cara, N.N. Albanese, F. Costantini, M.R. Marabeti, R. Musso, C. Lupo, E. Roz, I. Pucci-Minafra, Large-scale proteomic identification of S100 proteins in breast cancer tissues, BMC Cancer 10 (2010) 476.
[16] R.L. Eckert, A.M. Broome, M. Ruse, N. Robinson, D. Ryan, K. Lee, S100 proteins in the epidermis, J. Invest. Dermatol. 123 (2004) 23–33.
[17] Y. Tutar, Dimerization and ion binding properties of S100P protein, Protein Pept. Lett. 13 (2006) 301–306.
[18] H. Zhang, G. Wang, Y. Ding, Z. Wang, R. Barraclough, P.S. Rudland, D.G. Fernig, Z. Rao, The crystal structure at 2A resolution of the Ca2+ -binding protein S100P, J. Mol. Biol. 325 (2003) 785–794.
[19] M. Koltzscher, V. Gerke, Identification of hydrophobic amino acid residues involved in the formation of S100P homodimers in vivo, Biochemistry 39 (2000) 9533–9539.
[20] H. Kawasaki, S. Nakayama, R.H. Kretsinger, Classification and evolution of EF-hand proteins, Biometals 11 (1998) 277–295.
[21] M. Laible, K. Boonrod, Homemade site directed mutagenesis of whole plasmids, J. Vis. Exp. (2009).
[22] A.S. Kazakov, A.S. Sokolov, A.A. Vologzhannikova, M.E. Permyakova, P.A. Khorn, R.G. Ismailov, K.A. Denessiouk, A.I. Denesyuk, V.A. Rastrygina, V.E. Baksheeva, E.Y. Zernii, D.V. Zinchenko, V.V. Glazatov, V.N. Uversky, T.A. Mirzabekov, E.A. Permyakov, S.E. Permyakov, Interleukin-11 binds specific EF-hand proteins via their conserved structural motifs, J. Biomol. Struct. Dyn. 35 (2017) 78–91.
[23] C.N. Pace, F. Vajdos, L. Fee, G. Grimsley, T. Gray, How to measure and predict the molar absorption-coefficient of a protein, Protein Sci. 4 (1995) 2411–2423.
[24] H.E. Blum, P. Lehky, L. Kohler, E.A. Stein, E.H. Fischer, Comparative properties of vertebrate parvalbumins, J. Biol. Chem. 252 (1977) 2834–2838.
[25] S.E. Permyakov, A.A. Vologzhannikova, V.I. Emelyanenko, E.L. Knyazeva, A.S. Kazakov, Y.S. Lapteva, M.E. Permyakova, A.P. Zhadan, E.A. Permyakov, The impact of alpha-N-acetylation on structural and functional status of parvalbumin, Cell Calcium 52 (2012) 366–376.
[26] M. Hackel, H.J. Hinz, G.R. Hedwig, Partial molar volumes of proteins: amino acid side-chain contributions derived from the partial molar volumes of some tripeptides over the temperature range 10-90 degrees C, Biophys. Chem. 82 (1999) 35–50.
[27] M. Häckel, H.J. Hinz, G.R. Hedwig, A new set of peptide-based group heat capacities for use in protein stability calculations, J. Mol. Biol. 291 (1999) 197–213.
[28] S.E. Permyakov, A.G. Bakunts, M.E. Permyakova, A.I. Denesyuk, V.N. Uversky, E.A. Permyakov, Metal-controlled interdomain cooperativity in parvalbumins, Cell Calcium 46 (2009) 163–175.
[29] N. Sreerama, S.Y. Venyaminov, R.W. Woody, Estimation of protein secondary structure from circular dichroism spectra: inclusion of denatured proteins with native proteins in the analysis, Anal. Biochem. 287 (2000) 243–251.
[30] V.N. Uversky, Use of fast protein size-exclusion liquid chromatography to study the unfolding of proteins which denature through the molten globule, Biochemistry 32 (1993) 13288–13298.
[31] F.J. Farris, G. Weber, C.C. Chiang, I.C. Paul, Preparation, crystalline structure and optical properties of the fluorescent probe, 4-4-bis-1-phenylamino-8-naphthalene sulfonate, J. Am. Chem. Soc. 100 (1978) 4469–4474.
[32] E.A. Burstein, V.I. Emelyanenko, Log-normal description of fluorescence spectra of organic fluorophores, Photochem. Photobiol. 64 (1996) 316–320.
[33] S.E. Permyakoy, A.G. Bakunts, A.I. Denesyuk, E.L. Knyazeva, V.N. Uversky, E.A. Permyakov, Apo-parvalbumin as an intrinsically disordered protein, Proteins 72 (2008) 822–836.
[34] K. Peng, S. Vucetic, P. Radivojac, C.J. Brown, A.K. Dunker, Z. Obradovic, Optimizing long intrinsic disorder predictors with protein evolutionary information, J. Bioinform. Comput. Biol. 3 (2005) 35–60.
[35] Z.L. Peng, L. Kurgan, Comprehensive comparative assessment of in-silico predictors of disordered regions, Curr. Protein Pept. Sci. 13 (2012) 6–18.
[36] X. Fan, L. Kurgan, Accurate prediction of disorder in protein chains with a comprehensive and empirically designed consensus, J. Biomol. Struct. Dyn. 32 (2014) 448–464.
[37] K. Peng, P. Radivojac, S. Vucetic, A.K. Dunker, Z. Obradovic, Length-dependent prediction of protein intrinsic disorder, BMC Bioinformatics 7 (2006) 208.
[38] P. Romero, Z. Obradovic, X. Li, E.C. Garner, C.J. Brown, A.K. Dunker, Sequence complexity of disordered protein, Proteins 42 (2001) 38–48.
[39] Z. Dosztanyi, V. Csizmok, P. Tompa, I. Simon, IUPred: web server for the prediction of intrinsically unstructured regions of proteins based on estimated energy content, Bioinformatics 21 (2005) 3433–3434.
[40] B. Xue, R.L. Dunbrack, R.W. Williams, A.K. Dunker, V.N. Uversky, PONDR-FIT: a meta-predictor of intrinsically disordered amino acids, Biochim. Biophys. Acta 1804 (2010) 996–1010.
[41] J. Prilusky, C.E. Felder, T. Zeev-Ben-Mordehai, E.H. Rydberg, O. Man, J.S. Beckmann, I. Silman, J.L. Sussman, FoldIndex: a simple tool to predict whether a given protein sequence is intrinsically unfolded, Bioinformatics 21 (2005) 3435–3438.
[42] B. He, K. Wang, Y. Liu, B. Xue, V.N. Uversky, A.K. Dunker, Predicting intrinsic disorder in proteins: an overview, Cell Res. 19 (2009) 929–949.
[43] Z. Peng, L. Kurgan, On the complementarity of the consensus-based disorder prediction, Pac. Symp. Biocomput. (2012) 176–187.
[44] F. Meng, V.N. Uversky, L. Kurgan, Comprehensive review of methods for prediction of intrinsic disorder and its molecular functions, Cell. Mol. Life Sci. 74 (2017) 3069–3090.
[45] F. Meng, V. Uversky, L. Kurgan, Computational prediction of intrinsic disorder in proteins, Curr. Protoc. Protein Sci. 88 (2017) 2 16 11-12 16 14.
[46] I. Walsh, M. Giollo, T. Di Domenico, C. Ferrari, O. Zimmermann, S.C. Tosatto, Comprehensive large-scale assessment of intrinsic protein disorder, Bioinformatics 31 (2015) 201–208.
[47] G.V. Semisotnov, N.A. Rodionova, O.I. Razgulyaev, V.N. Uversky, A.F. Gripas, R.I. Gilmanshin, Study of the "molten globule" intermediate state in protein folding by a hydrophobic fluorescent probe, Biopolymers 31 (1991) 119–128.
[48] L. Shi, D.R. Palleros, A.L. Fink, Protein conformational changes induced by 1,1'-bis (4-anilino-5-naphthalenesulfonic acid): preferential binding to the molten globule of DnaK, Biochemistry 33 (1994) 7536–7546.
[49] L. Stryer, The interaction of a naphthalene dye with apomyoglobin and apohemoglobin. A fluorescent probe of non-polar binding sites, J. Mol. Biol. 13 (1965) 482–495.
[50] E.A. Permyakov, V.N. Uversky, Fluorescence spectroscopy of intrinsically disordered proteins, in: V.N. Uversky, S. Longhi (Eds.), Instrumental Analysis of Intrinsically Disordered Proteins: Assessing Structure and Conformation, John Wiley & Sons, Inc., Hoboken, New Jersey, 2009, pp. 323–344.
[51] A.V. Gribenko, G.I. Makhatadze, Oligomerization and divalent ion binding properties of the S100P protein: a Ca2+/Mg2+-switch model, J. Mol. Biol. 283 (1998) 679–694.